THE AMERICAN SOCIETY OF MECHANICAL ENGINEERS
345 E. 47th St., New York, N.Y. 10017

95-GT-343

DEVELOPMENT AND APPLICATION OF A MULTISTAGE NAVIER-STOKES FLOW SOLVER PART II: APPLICATION TO A HIGH PRESSURE COMPRESSOR DESIGN

C. R. LeJambre
R. M. Zacharias
B. P. Biederman
A. J. Gleixner
C. J. Yetka

Pratt & Whitney
E. Hartford, CT

ABSTRACT

Two versions of a three dimensional multistage Navier-Stokes code were used to optimize the design of an eleven stage high pressure compressor. The first version of the code utilized a "mixing plane" approach to compute the flow through multistage machines. The effects due to tip clearances and flowpath cavities were not modeled. This code was used to minimize the regions of separation on airfoil and endwall surfaces for the compressor. The resulting compressor contained bowed stators and rotor airfoils with contoured endwalls. Experimental data acquired for the HPC showed that it achieved 2% higher efficiency than a baseline machine, but it had 14% lower stall margin. Increased stall margin of the HPC was achieved by modifying the stator airfoils without compromising the gain in efficiency as demonstrated in subsequent rig and engine tests. The modifications to the stators were defined by using the second version of the multistage Navier-Stokes code, which models the effects of tip clearance and endwall flowpath cavities, as well as the effects of adjacent airfoil rows through the use of "bodyforces" and "deterministic stresses". The application of the Navier-Stokes code was assessed to yield up to 50% reduction in the compressor development time and cost.

INTRODUCTION

The design system for compression systems at Pratt & Whitney has evolved since the 1940's. Through the 1950's, the design system was based on one dimensional fluid dynamics. By the 1960's design technology had advanced to two dimensional, inviscid, steady flow, when streamline throughflow calculations were used and the 2D blading was based on correlations derived from a cascade test data base. In the 1970's blade-to-blade potential flow solvers were introduced with simple boundary layer model calculations. The potential flow solvers were used to optimize the 2D blading. By the 1980's viscous effects were accounted for though the solution of the two dimensional Navier-Stokes equations. However, neither the CFD codes nor the computers available to designers were advanced enough to routinely solve 3D problems for design studies. Empirical correlations were applied to account for 3D endwall, tip clearance and cavity and bleed effects. These correlations were based on the data base developed by commercial engine companies, universities, research laboratories, etc. Final blading was only designed from 20% to 80% span; the empirical design rules determined the blading near the endwalls. However, the design rules broke down in the viscous regions of the problem (on the airfoil surface and in the endwalls) when drastic changes were made to the airfoil geometries because these rules did not fundamentally describe the three dimensional, viscous aerodynamics of compressor flows.

The development and introduction of novel, three dimensional blading concepts to optimize the compressor performance was expensive and time consuming. It was limited to small, incremental changes to heavily tested designs because the risk associated with implementing significant changes in airfoil designs was high. A typical high pressure compressor design proceeded as follows, as depicted in Fig. 1. Overall flow and pressure rise for the compressor was defined. Number of stages and flowpath were chosen, and velocity triangles were created using a meanline program. Preliminary blading was defined using a streamline program with empirical corrections for 3D viscous effects. 2D airfoil cross sections were defined and stacked to form the 3D airfoil. Simple 2D viscous CFD calculations were made on representative airfoil cross sections to check blade loadings, flow separations, etc. A research rig was then built to test the configuration. This rig usually contained one third of the total number of stages and used variable pitch geometry in order to properly match the stages and refine vane and blade incidences. After the research rig program was completed, a full-size compressor rig test program was undertaken with variable geometry in all stages, again to allow for fine tuning in order to match stages and achieve the design flow capacity and work distributions. Finally, engine hardware was defined and built for a full scale engine test.

Presented at the International Gas Turbine and Aeroengine Congress and Exposition
Houston, Texas - June 5-8, 1995

The design was assessed after each step subsequent to the meanline program, and could be changed.

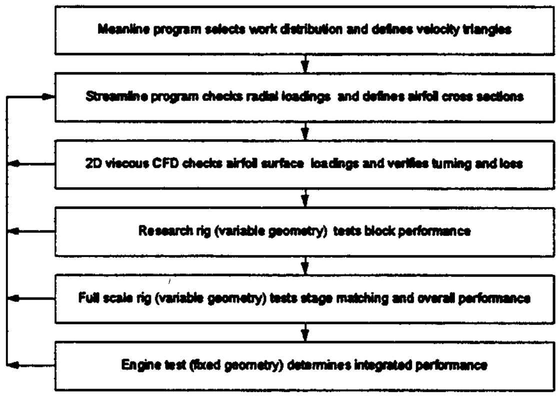

Figure 1. Empirically based design system.

This iterative procedure would typically take up to three years to carry out and cost as much as twenty million dollars. However, the resulting design was not optimum. No detailed understanding of the internal fluid mechanics was gained; it was not yet possible to break from a previous design with any confidence and in a cost effective manner since the empirically based design system did not extend beyond the data base of tested geometries.

The long development time, high cost and limited performance gains associated with this design system hastened the development of a new design technology based on the full three dimensional equations of motion. Design methods based on solving the Navier-Stokes equations became accurate and practical in the 1990's for isolated cascades of airfoils such as fans (Rhie, 1994). Early work in developing multistage turbomachinery CFD was done by researchers such as Ni (1989), Dawes (1992), Denton (1992), Adamczyk (1990), Chima (1991), Hah (1991), and Jennions (1993). As computers became more powerful, it became practical to routinely solve multiple rows of airfoils in order to evaluate new design concepts. This allowed designers to progressively replace the empirical correlations with physics-based models, which resulted in the successful introduction of new three dimensional blading concepts in the compressor design.

This paper will discuss the application of two versions of a Navier-Stokes based computational fluid dynamics (CFD) design system to high pressure compressor design. Version I was a multistage code that was a simple extension of the isolated blade row technique, where boundary conditions were applied at mid-gap locations, and a mixing plane model was used. It will then discuss the application of Version II, where the code was improved by using bodyforces and deterministic stresses to more accurately account for the effects of neighboring airfoils. It will illustrate how designers used CFD as a "numerical rig" in order to conduct "numerical experiments" and interrogate new physical concepts when optimizing new blading concepts. This paper will discuss the application of the new design system to a new high compressor design, including the optimization of bowed stators and controlled diffusion rotor endwalls in a multistage environment. The role of CFD in understanding stage matching and the impact of managing radial flow distributions will be discussed. The philosophy of using CFD models to guide the development process from design through test will be stressed (Rubbert, 1994). The resulting reduction in development cost and time, and the increase in compressor performance will be shown.

NAVIER-STOKES BASED DESIGN SYSTEM

As CFD and computer hardware technology advanced in the late 1980's and early 1990's, it became possible to routinely compute 3D viscous flowfields for compressor cascades. Development of isolated airfoil row CFD models (Rhie,1994) and subsequent development of multistage CFD models, coupled with the implementation of parallel CFD algorithms on networked engineering workstations (Fischberg, 1995, Gundy-Burlet, 1991, and Blech., 1992) made it possible for compressor designers to conduct extensive development programs numerically rather than experimentally. These technologies would become the basis of the 1990's design system.

A goal was defined to create a new design system that centered around 3D Navier-Stokes calculations for multistage compressor flows. The 3D CFD would be used to assess the performance of the compressor instead of the research rig tests and full scale rig tests with variable stator geometry. The objective of the design system was to go to full scale rig test with engine hardware. The goal was to cut the design cycle costs and time by up to 50%, while increasing the performance of the compressor. The new design system is depicted in Fig. 2.

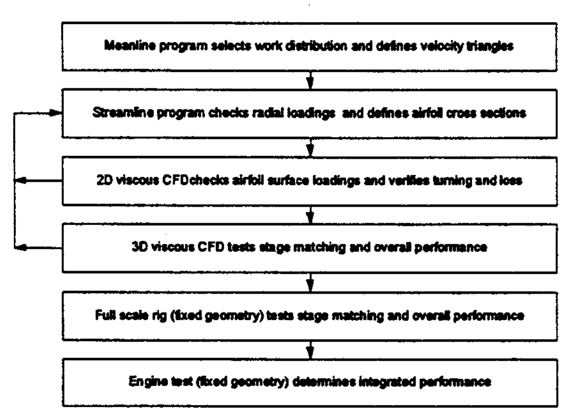

Figure 2. New design system centers around 3D Navier-Stokes calculations instead of rig testing.

A new design system based on 3D Navier-Stokes analysis was designed as follows. Preliminary flowpath shape and size, and preliminary blading was defined using the 1D and 2D meanline and streamline models with empirically derived corrections. However, prior to undertaking any time consuming and expensive rig or engine testing, the design is extensively tested using a 3D multistage Navier-Stokes CFD code. This code is described in the companion paper entitled "Development and Application of a Multistage Navier-Stokes Flow Solver, Part I: Multistage Modeling Using Bodyforces and Deterministic Stresses", and will be briefly reviewed in a later section.

By using the 3D Navier-Stokes procedure to assess the performance of the new design, the designer would be able to properly "match" stages to achieve design pressure rise and flow characteristics more quickly and less expensively than a rig program. Design rules based on empiricism would be replaced with physics-based models derived from the CFD calculation. The choice to model or grid additional physical features was based on the computational resources required. It was determined that gridding and computing the bleed ports and the stator cavities required the same amount of grid as the airfoil passage (approximately 300,000 grid points). Using a total of 600,000 grid points per blade row would not be possible for a production design system, so it was decided to model the bleed and the cavity through flow extraction/injection techniques. However, it was determined through calibration that the tip clearance region of rotor tips could be accurately gridded and computed by adding 10% more grid.

Using the new design system, detailed understanding of the fluid flow would be obtained in three dimensions; the flowfield would be computed to the blade surface and to the endwalls, and sources of blockage and loss such as tip clearance, cavities, bleeds, and airfoil separation would be simulated and understood more accurately than by the empirically based models.

In the new Navier-Stokes based design system, 3D blockage/loss effects would be accounted for in the design, and novel 3D blading concepts could be implemented to maximize performance. In addition, the off-design performance of the compressor could be assessed; the effect of flow migration on off design performance can be simulated and understood, and could therefore be taken into account in the design. With proper validation, the Navier-Stokes based design system would be used to extend designs beyond the current experience envelope. These new 3D designs would be developed and refined in a cost effective manner, which would greatly impact the compressor design cycle cost, time and performance.

Developing and implementing this new design system was an ambitious goal. It was understood by all involved that the system would have to *evolve*; the degree of accuracy required for design assessment would need to be defined, and the requirement to model real-life features such as rotor tip clearances, variable pitch stator endgaps, stator cavities, and bleeds was unknown. It was therefore decided to develop the system in conjunction with a new eleven stage high compressor design. The data acquired during testing would be used to guide the development of the CFD based design system.

NASTAR CODE

The NASTAR code was the 3D Navier-Stokes solver chosen for use in the new multistage compressor design system, and is described in the companion paper by Rhie and in Rhie, 1988. Important features required for the accurate and economical design computation of compressor flows are described in this section.

The NASTAR code is a finite volume, implicit, pressure correction Reynolds-averaged Navier-Stokes solver. It uses the standard two equation $\kappa - \varepsilon$ turbulence model integrated to the wall to resolve the viscous boundary layer. The code is parallelized to run on a network of engineering workstations. Each blade row is solved on a computational mesh containing approximately 300,000 points using a standard single block H-mesh.

NASTAR utilizes a grid point "flagging" system which allows for specific boundary conditions to be applied at a given grid node. A flag is an integer value associated with each grid node that denotes the boundary condition to be applied. Examples include viscous wall, symmetry plane, periodic boundary, mass flow injection or extraction, and flow obstruction (Rhie, 1994). The flag system allows for geometric details, such as rotor tip clearances and variable pitch stator endgaps to be easily incorporated into the computational model.

Figures 3 and 4 show details of the computational mesh for a rotor with tip clearance and a variable pitch stator with endgaps. In these models, mesh points are placed within the airfoil and the flag system is used to describe which points are "solid metal" and which points are "fluid". Careful grid stretchings ensure that boundary layers are properly represented; the first grid point off of a solid surface is typically placed at a y+ value of 1.0. A hyperbolic tangent stretching function is used to distribute grid points away from the wall. The stretching function forces the second grid point off of the wall to be placed at a y+ value of 2.0.

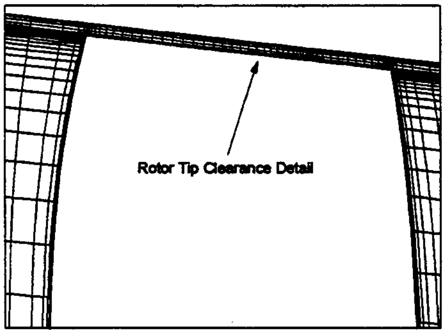

Figure 3. Detail of grid at rotor tip.

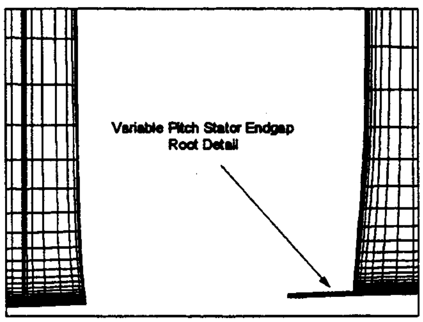

Figure 4. Grid detail near variable pitch stator root, showing blunt trailing edge at trunnion trailing edge.

Other advantages of the flagging system allow for the inclusion of simple stator cavity and endwall bleed models. The cavity and bleed models are simple flow extraction/injection models added to the 3D Navier-Stokes solution which provide local streamline curvature effects.

Figure 5 shows a schematic of the cavity model. The cavity flow, which is driven by the trailing edge to leading edge pressure gradient, the disk pumping of the drum rotor, and the losses through the knife-edge seals, is modeled as flow extraction at the trailing edge and injection at the leading edge. The driving pressure gradient is extracted from the CFD solution and the pumping and loss through the cavity is driven by a 1D model that accounts for knife edge seal clearance, drum rotor speed, and cavity depth. The model prescribes a cavity flow rate, which is extracted at the stator trailing edge and re-injected at the leading edge. The mass flux is applied uniformly over the extraction and injection slots. The flow solver adjusts the total pressure at the injection location until the prescribed mass flow is achieved. It also prescribes re-injection total temperature boundary at the leading edge. The static pressure at the flow extraction locations near the trailing edge is varied by the solver until the prescribed mass flow rate is achieved. The flow re-injection at the leading edge of the stator creates loss and blockage which is then accounted for in the 3D solution procedure.

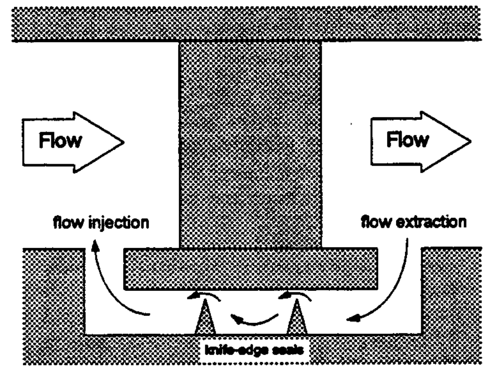

Figure 5. Schematic of cavity model.

Figure 6 shows a schematic of the bleed model. The bleed flow is extracted from the calculation through an orifice carved out of the computational mesh. This flow extraction is required to properly compute the flow angles into the next airfoil row, because the bleed changes the corrected flow into the next row. As in the cavity model, the mass is extracted uniformly over the orifice. The code treats this zone as an exit boundary condition and varies the local static pressure until the prescribed mass flow extraction is achieved.

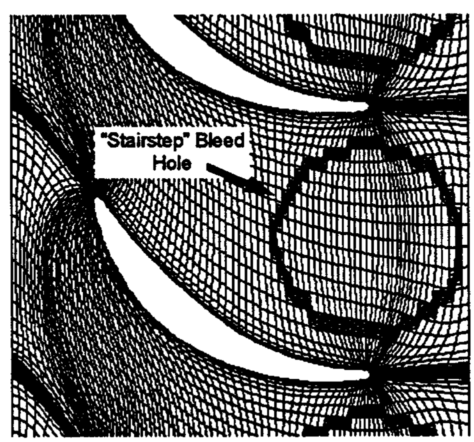

Figure 6. Grid detail showing model of bleed hole.

The multistage NASTAR code was developed in two versions. In the first, the multistage environment was accounted for by using a "mixing plane" approach. This approach was satisfactory at the design point when flow separations were small. It is shown in the companion paper that the mixing plane model tends to overemphasize the effects of upstream blade row separation on the downstream blade row. The large blockages created upstream are not mixed out properly as they are in the second version, where the multistage environment is accounted for through the use of bodyforce and deterministic stress models (see companion paper by Rhie and Adamczyk, 1989). This approach was developed to allow for analysis off-design, where flow separations become significant and the deterministic stresses tend to mix out the blockages of the upstream blade row.

The first version of the code was a simple extension of the isolated blade row NASTAR code. The total pressure, total temperature, and flow angles are given and held upstream of the first airfoil row. The static pressure is given and held downstream of the last blade row. Intermediate blade rows apply the total pressure, total temperature, and flow angles midway between the trailing edge of the upstream row and the current leading edge. These conditions are convected from upstream through a mixing plane (Dawes, 1992) to account for reference frame changes. The static pressure is applied midway between the current trailing edge and the leading edge of the downstream blade row.

The second version of the code improved the multistage modeling. In this version, multistage effects are modeled through the use of bodyforces and deterministic stresses. As in the first version, far upstream conditions are given and held. Similarly, static pressure is specified far downstream. The difference between the two versions has to do with the way information is passed between intermediate blade rows, and how neighboring blade rows effect an intermediate blade row.

Figure 7 shows a side view (axial-radial projection) of a typical computational mesh for a compressor stage. The top figure is the computational domain for the stator, while the bottom figure is for the downstream rotor. The stator mesh and computation has several features. First, since this is a stage from the front block of the compressor which contains variable pitch stators, the stator endgap clearances are gridded. A side view detail of the stator endgap at the inner diameter was shown in Figure 4. The stator domain contains an axial extension which encompasses the downstream rotor. The grid in this region conforms to the geometry of the rotor, and is used to model the back-pressuring effects of the rotor. Pressure forces developed in the rotor computational domain are transferred to the stator domain and are applied as axisymmetric bodyforce source terms. Deterministic stresses due to circumferentially non-uniform flow in the stator domain are computed and transferred as turbulence-like stresses to the rotor domain.

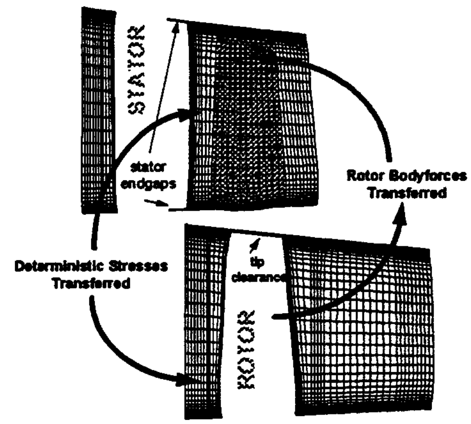

Figure 7. Multistage modeling in NASTAR includes incorporation of bodyforces through transfer of blade forces.

The rotor mesh and computation has several features. The rotor tip clearance is gridded. A detail of the clearance grid was shown in Figure 4. Airfoil pressure forces computed on the rotor are axisymmetrically passed to the upstream stator, while deterministic stresses caused by upstream stator flowfield circumferential non-uniformities are imposed on the rotor flowfield. Circumferential non-uniformities caused by the rotor (due to leading edge bow shocks, for example) are passed upstream and overlaid on top of the stator as deterministic stresses.

APPLICATION TO HIGH PRESSURE COMPRESSOR DESIGN

The new Navier-Stokes based design system was developed and used to design and optimize a new high pressure compressor configuration. The new design was for a growth version of a current high thrust engine, and as such, was required to fit within several pre-established geometric and aerodynamic constraints. It had to match and perform with other engine components such as the low pressure compressor and the high pressure turbine. Also, since the growth engine designs are limited by thermal/mechanical design constraints, high compressor efficiency improvements were required to stay within material thermal limits. In this case, the efficiency improvements were less important for fuel burn performance. The goal of the design was to improve high pressure compressor effficiency without sacrificing stall margin.

New technologies were available and were well understood in an isolated environment for improving the high compressor efficiency, such as bowed stators and controlled diffusion rotor root endwalls, but they were not well understood in the multistage environment. The empirically based design system did not account for these fundamental changes in blading in its blockage/loss/turning models. The impact of radical flow redistribution through blading changes introduced a substantial risk in terms of off design stability performance. The traditional cycle of design/test/redesign would have taken too long, been too expensive and would have involved too much risk to have a timely impact on growth engine development using these technologies. The Navier-Stokes based design system was developed to understand and tailor the radial and axial flows, and to optimize the new blading technology to gain efficiency without sacrificing stability.

DESIGN/OFF DESIGN ANALYSIS AND TEST PROGRAM

This section describes the analysis and CFD system development that was performed in support of the new high pressure compressor design.

The initial blading design/optimization was carried out with the earliest versions of the multistage NASTAR code. This version used a simplistic interrow mixing plane model to pass the calculated exit conditions of one row to the inlet of the next. This multistage technique was adequate for the designer to optimize 3D blading features (stator bow and rotor root contouring) in order to eliminate / minimize flow separations. It was anticipated that the elimination of flow separation would account for the majority of the required efficiency improvment.

One of the new airfoil contouring technologies employed to eliminate flow separations was bowed stators. An example of how NASTAR was used to understand the physics of bowed stator technology is described. Figure 8 shows a perspective view of a typical middle block straight (2D) stator. Air flow enters from the right as indicated. The corner separations on the suction surface of the endwall are indicated by the iso-surfaces of zero axial flow. The flow within this surface is separated, and is a source of blockage, loss and turning deviation. Figure 9 shows a bowed stator. The effect of the bow is to produce radial forces which drive flow into the corners, and eliminate the corner separations. The iso-surfaces of zero axial flow (the envelope of flow separation) is substantially reduced, which reduces the loss and blockage associated with the stator. Additionally, the deviation of flow angle from metal angle has been changed. The aerodynamic impact of stator bowing is well known (Weingold, 1995) and was not developed during this design. However, the *interaction* of the bowed stator with its neighboring airfoil rows was not well understood, and was not accounted for in the loss, blockage and turning empiricisms. The 3D Navier-Stokes design system allowed designers to *optimize* the bowed stator design in the multistage design-point/off-design environment.

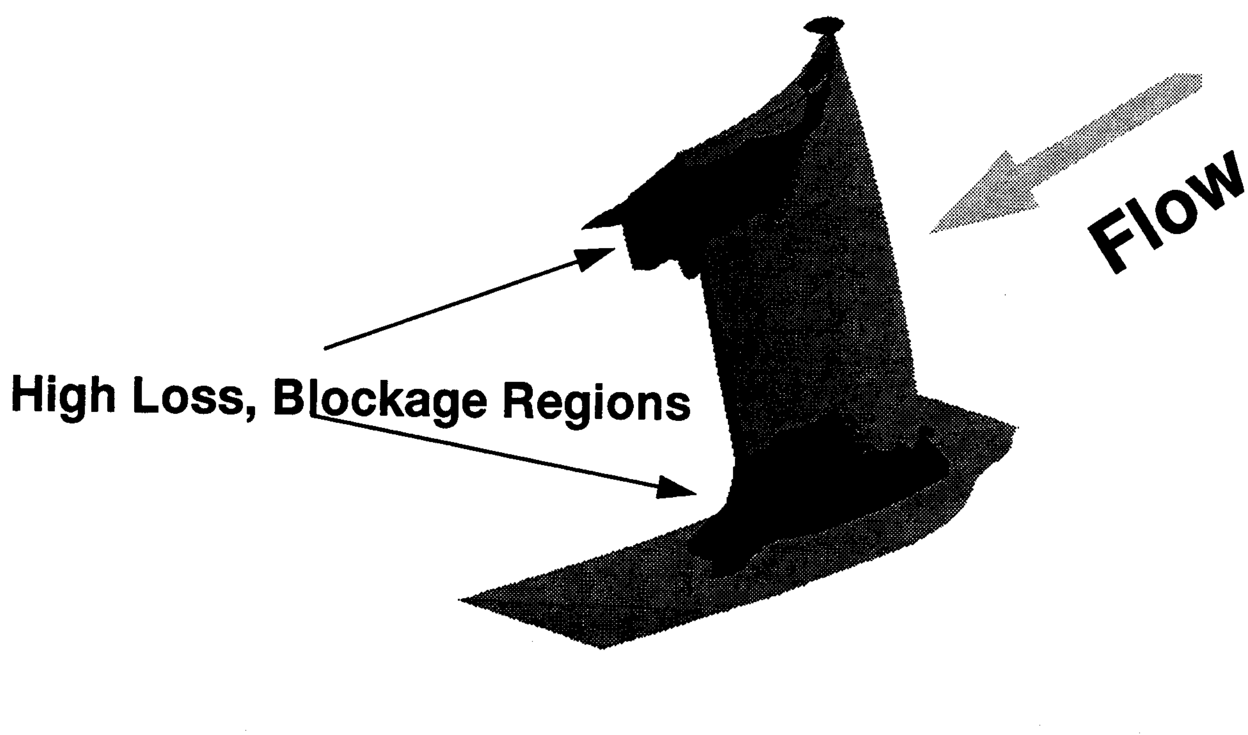

Figure 8. Iso-surface of zero axial flow, showing boundary of 3D separation evident in corners of straight compressor stators.

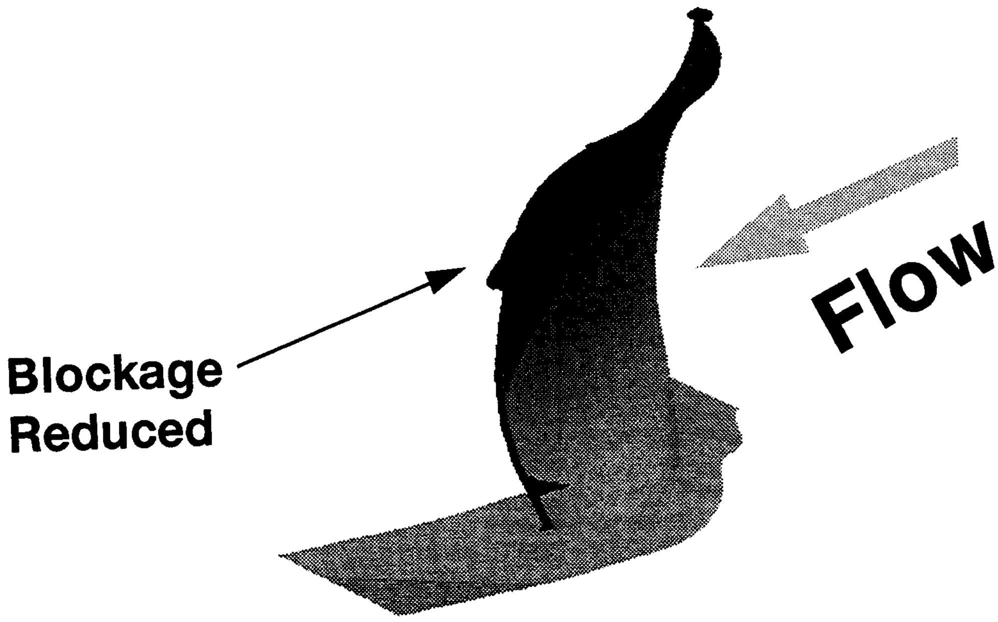

Figure 9. Iso-surface of zero axial flow, showing reduction of 3D separation in bowed compressor stators.

The quantitative effect of bowing the stators is shown in Figures 10 and 11. Figure 10 is a plot of the circumferentially mass averaged radial profiles of axial velocity at the stator trailing edge. Both stators were run to the same mass flow rate. The figure shows regions of low axial velocity near the root and the tip for the straight stator. This region of blockage forces flow to the mid-span region, where the average axial velocity is higher than the bowed stator.

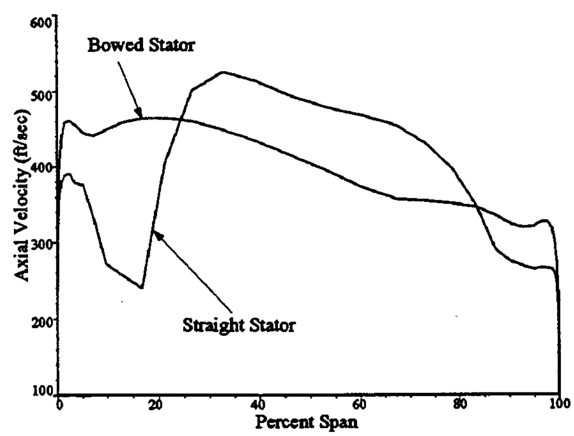

Figure 10. Straight stators show regions of low axial velocity in the endwalls, and a region of high axial velocity in the midspan, compared to bowed stators.

The effect of stator bowing on average stator exit flow angle is shown in Figure 11. The circumferentially mass averaged axial and tangential velocity components were used to compute the average flow angle. Purely axial flow would show a flow angle of 90 degrees. The figure shows a severe flow angle falloff in the endwalls of the straight stator, compared to the bowed stator. The large change in stator exit flow angle that occurs when switching from straight to bowed stators forced the designers to alter the rotor leading edge camber angle to properly match the stage. The 3D viscous CFD was used to accomplish this match.

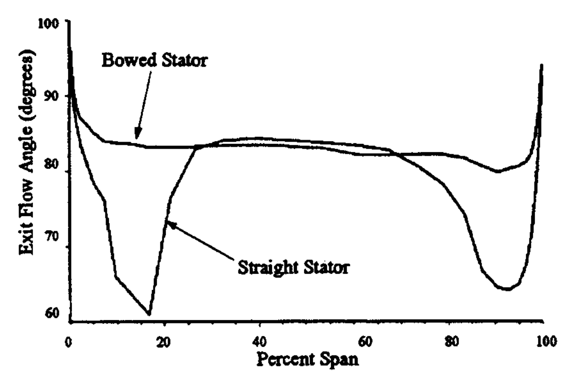

Figure 11. Effect of stator bow is to change average stator exit flow angle distribution.

Similar optimization of rotor endwall contouring concepts was achieved using NASTAR. Rotor root contouring, sometimes (mistakenly) referred to as 'area-ruling', was intially employed in the design as a means of increasing the 'choke-margin' of high Mach number rotors. This was required to offset the increased airfoil thicknesses required to improve airfoil durability at higher mechanical speeds. The resulting shape of the ID flowpath wall has additional benefits in that it creates a radial force much the same as stator bow. This radial force redistributes flow and reduces the tendency of the flow to separate at the intersection of the airfoil suction surface and ID flowpath wall. Figure 12 compares the ID wall static pressures of a contoured and non-contoured rotor operating with identical inlet conditions. Figure 13 compares near suction surface and blade to blade streaklines of a typical rotor with non-contoured and countoured ID flowpaths. The separations near the ID wall are completely eliminated with contouring. The remaining separations outboard of the ID wall are due to high 2D airfoil surface loading.

The contoured root not only eliminated separations but has allowed for increased diffusion. This effect, if not accounted for in the design, becomes significant after several compressor stages and can cause the radial total pressure profile to deviate from the design intent. The 3D viscous code was used to optimize the root contour shape and quantify its impact in the multistage environment.

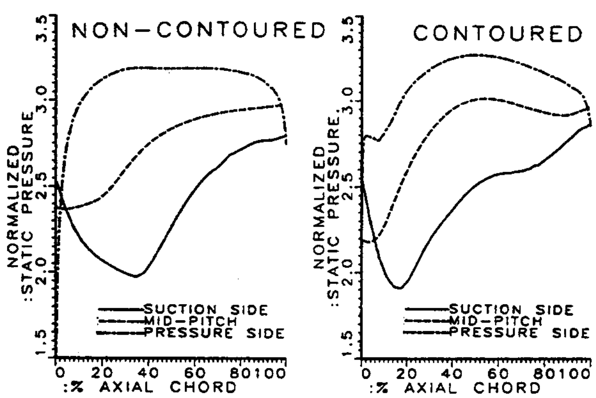

Figure 12. Comparison of ID wall static pressure for conventional and contoured rotor endwalls.

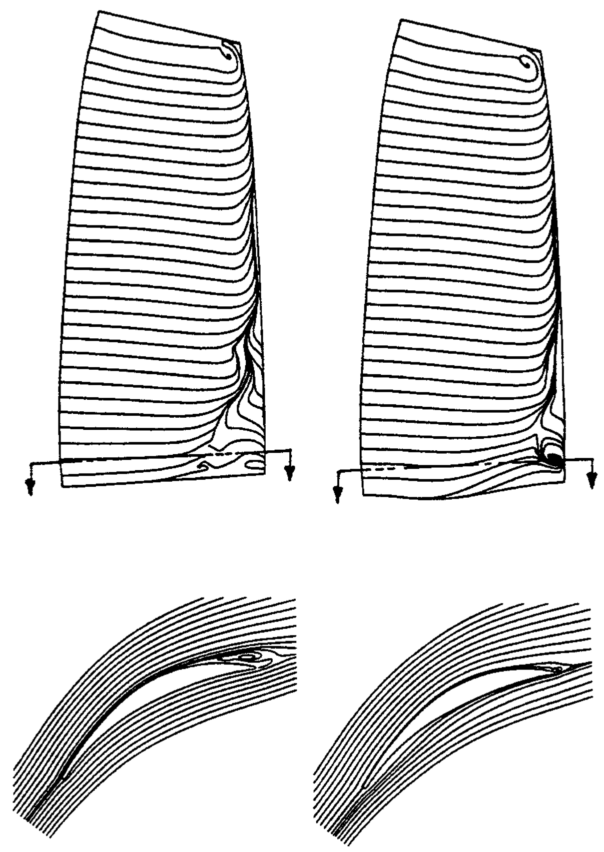

Figure 13. Streaklines comparing separation near rotor suction surface and near rotor root.

Individual stator / rotor stage pressure ratio / flow capacities were calculated and compared to design intent. Airfoil trailing edge cambers were adjusted based on the initial calculation to achieve the desired flow/pressure ratio levels. Airfoil leading edge angles were also optimized to position each section at the minimum incidence-loss point.

Stator bow angle and radial extent were varied to eliminate endwall corner separations while maintaining unseparated core sections. The depth and chordwise location of the rotor root contouring was also optimized to eliminate separations. Estimates based on these early multistage Navier-Stokes calculations indicated overall compressor efficiency could be improved by as much as 2%.

The iterative blade design / Navier-Stokes analysis process was completed within three months of design start, and final blading definition was released for airfoil fabrication. As mentioned earlier in this paper these airfoils were manufactured with the intent of being directly substituted into development engine compressors. The initial performance however, was to be demonstrated in a full eleven stage high pressure compressor rig. This design using the first version of NASTAR concentrated on increasing performance at the design point. Effects such as tip clearance, stator endgaps, and cavities and bleeds were not modeled. It was not known, however, how the new compressor would perform at off-design conditions, when separations become larger and clearance and cavity flows potentially become more important.

Figure 14 shows a cross section of the NASTAR compressor flowpath and blading. As shown in Table 1 the design point of the NASTAR compressor is identical to the baseline compressor. Beside the solidity increase the only major features incorporated in the new design were bowed stators and contoured rotor roots

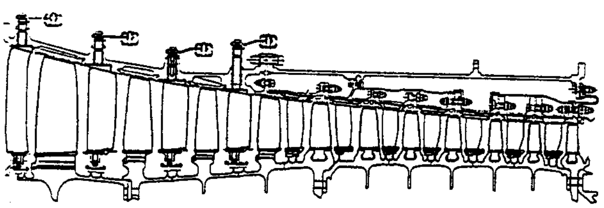

Figure 14. NASTAR compressor cross section.

DESIGN POINT COMPARISONS

	BASELINE COMPRESSOR	NASTAR COMPRESSOR
INLET CORRECTED FLOW	120 LBS/SEC	120 LBS/SEC
PRESSURE RATIO	10:1	10:1
SOLIDITY		
ROTORS	1.095	1.201
STATORS	1.208	1.348
AXIAL MACH NUMBER		
INLET	0.54	0.54
EXIT	0.23	0.23
MEAN WHEEL SPEED	950 FT/SEC	950 FT/SEC

Table 1. Baseline vs. NASTAR designed compressor design point comparisons.

Rig Build 1

The eleven stage compressor rig achieved goal performance. Overall pressure rise/flow capacity was within 1% of design goal. Efficiency was improved by 2.0% over the baseline. This increased efficiency was attributed primarily to bowed stators and contoured rotor roots which substantially reduced endwall separations. The positive results obtained in this rig test were an important step in the validation of the Navier-Stokes based design system. This rig test is summarized in Figure 27, which is a plot of compressor efficiency vs. stall margin. An assessment of P&W's current state-of-the art is the shaded line; it shows that compressor efficiency can typically be traded for stall margin. The results of the first rig test can be seen in the upper left portion of the line.

However, the goals of the engine program required that this efficiency be maintained but at a higher level of stall margin. In the interim between release of the final airfoil coordinates and the first testing of the rig, improvements were being made to the NASTAR code. The data suggested that the decrease in the stall margin was due to a decrease in axial flow in the outer half of the compressor, which was causing the rotor tips to become overloaded. Figure 20 shows the measured axial velocity profile at the exit of the compressor at the operating point, and at 11% above the operating line. The figure shows the drop in tip axial flow at the higher operating line.

Calculations using the first verstion of NASTAR, run without bodyforces, deterministic stresses, rotor tip clearances, cavity or bleed models did not match test data at high operating lines. Version I used the mixing plane model, and tended to overestimate the effect of transferring blockage to the downstream blade row (as discussed in the companion paper). Version I also neglected the blockage-producing mechanisms of tip clearance and stator cavities. These effects made Version I unreliable for determining the cause of the surge margin deficit. The addition of more complete physical modeling, which included the above features, provided a better match with the rig data.

An example of how the addition of the cavity model impacted blockage and stage size is show in Figures 15 and 16.

Figure 15 is a plot of circumferentially averaged axial velocity versus span at the leading plane of a middle block stator. The re-injection of cavity leakage flow creates a blockage at the root, which causes the axial velocity the increase outboard of 25% span.

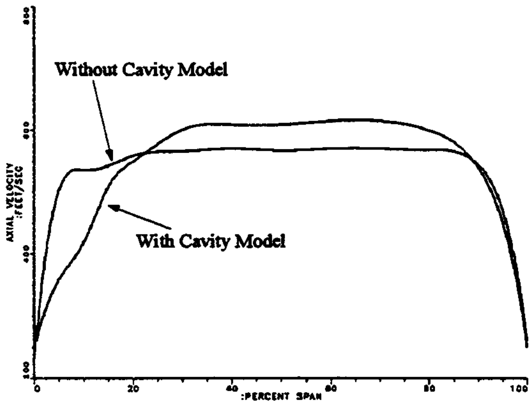

Figure 15. Cavity model produces blockage at the root of a stator leading edge.

This radial flow redistribution impacts the downstream rotor. The increase in axial flow delivers a more negative incidence to the rotor, which reduces the work done by the rotor. This effect can be seen in Figure 16, which shows the normalized, circumferentially averaged total pressure at the downstream rotor trailing edge plotted versus the span. The overall pressure rise for the case with the cavity model is reduced by 3% for this single stage.

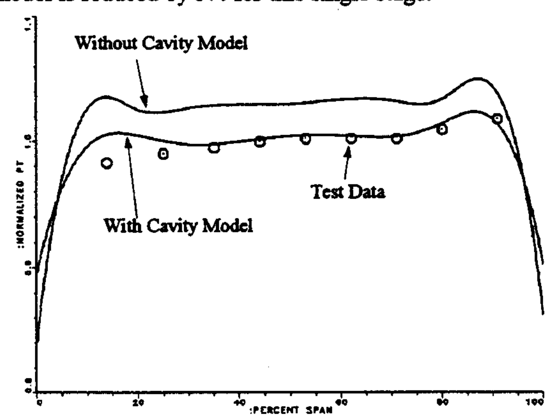

Figure 16. Cavity model causes pressure rise in downstream rotor to decrease.

Similarly, the effect of rotor tip clearance can impact the radial profiles downstream of the rotor. Figure 17 shows a mach number contour, in a blade-to-blade view, near the tip of a rotor computed with tip clearance. The effect of the tip leakage vortex on the mach number is clearly seen. This vortex creates loss which causes a total pressure falloff in the outer-diameter region of the rotor. As the compressor runs at higher operating lines closer to the stall limit, the leakage vortex responds by getting pushed farther upstream and creating more tip blockage. This effect is shown in Figure 18, which is the same rotor but run at a higher operating line The clearance vortex is pushed forward for the high opline case.

Figure 17 Rotor tip leakage vortex at opline condition.

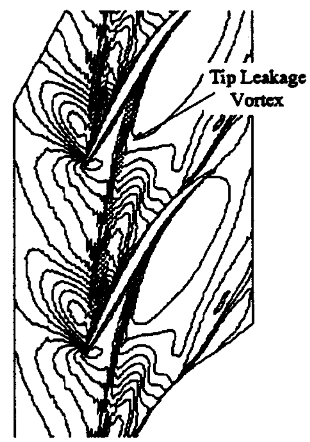

Figure 18. Tip leakage vortex at high opline condition, with vortex pushed forward.

Figure 19 shows how the tip clearance blockage increases as the rotor is backpressured. The figure plots the absolute change in circumferentially averaged axial velocity as a function of percent span. This figure is for the two cases depicted above. The figure shows that the change in axial velocity is greatest in the tip region, where the blockage due to the clearance vortex increases at the high operating line.

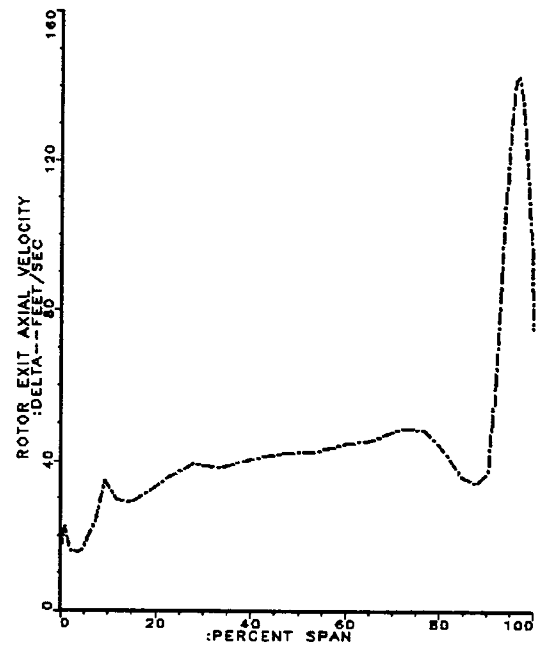

Figure 19. Rotor tip axial veolcity change increases with operating line.

By accounting for clearance flows, the designer also has a mechanism in which to determine the tip clearance sensitivity of the compressor by conducting numerical experiments with various tip clearance gap sizes.

Rig Build 2

Several options were identified to improve the basic compressor stall margin but these were limited by time and available hardware. A choice was made to re-operate existing blading in the middle stages of the compressor and to return to test. The re-operation of the mid-block blading consisted of removing a portion of the stator, or "cutting it back", near the root. A detailed explanation of how the cutbacks impact the radial flow distribution will be given in the following section "Rig Build 3".

The cutbacks were optimized using the second version of NASTAR. In this redesign, it was critical to predict the flowfield near stall, where separations become large and the mixing plane model breaks down. Here, proper transfer of blockage and the potential effects of neighboring blade rows are accounted for by the bodyforces and deterministic stresses. NASTAR was used to tailor the blading changes such that design point performance would not be compromised while improving the compressor's stall margin. The goal of the next rig test would then be to move horizontally to the right on Figure 27 and truly advance the state-of-the-art design.

The rig teardown, stator modifications and rig re-build was completed within three months of the previous build's conclusion. Test data indicated that the middle stage stator cutbacks were successful in improving stall margin without sacrificing design point performance. Figure 27 summarizes the second rig build. Stall margin was increased from 15% to 20%. The radial flow re-distribution suggested by the improved multistage NASTAR analysis was determined to be the source of this stability improvement. In fact, the continuing Navier-Stokes analysis suggested that even more improvements could be realized by extending this radial flow re-distribution philosophy further rearward in the compressor. Rear stage stator cutback redesigns were completed and blading modifications were called out.

Rig Build 3

The compressor rig was rebuilt with modified hardware and returned to test. This third and final rig test was successful; stall margin increased an additional 7% relative to the previous rig build and a modest gain in efficiency was also demonstrated. Figure 20 shows a typical stator modification used in both the NASTAR rig build 2 and NASTAR rig build 3 compressors. The local trailing edge root cutbacks were easily accomplished by simple reoperations of the existing stator airfoils. The results of the cutbacks are shown in figure 20. This figure compares the exit velocity profiles of the Build 1 and Build 3 compressors. These profiles are based on compressor exit pressure and temperature measurements and streamline throughflow calculations. As seen in the figure the radial flow redistributions accomplished by the cutbacks changed the off-design behavior of the compressor allowing substantial improvements in stall margin. Maintaining axial velocity near the tip has the desirable effect of offsetting the tip clearance vortex and delaying 'tip stall'.

Figure 27 summarizes the performance of this build. This rig data also showed that a new state-of-the-art of compressor design was achieved. The next step was to install this compressor directly into a development engine to verify its performance and stability in the engine environment.

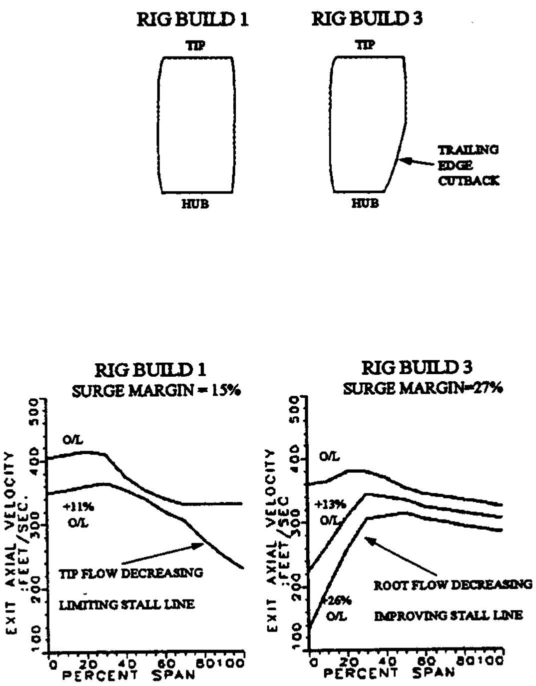

Figure 20. Stator cutback profiles and effect on radial profiles of axial velocity at compressor exit.

Figures 21-26 compare the measured rig total pressures and temperatures with the NASTAR calculation. The data is taken at the exit of each of the three compressor blocks; at the leading edge of stator 8 (front block exit), stator 12 (middle block exit), and compressor exit (rear block exit). Although the NASTAR calculation does not match the test data precisely, the calculation predicts the overall stage block pressure and temperature rise within 1%, which is within experimental accuracy. The ability of the code to produce solutions of this quality enabled the designers to proceed to the rig test with fixed engine hardware, rather than with variable pitch rig hardware.

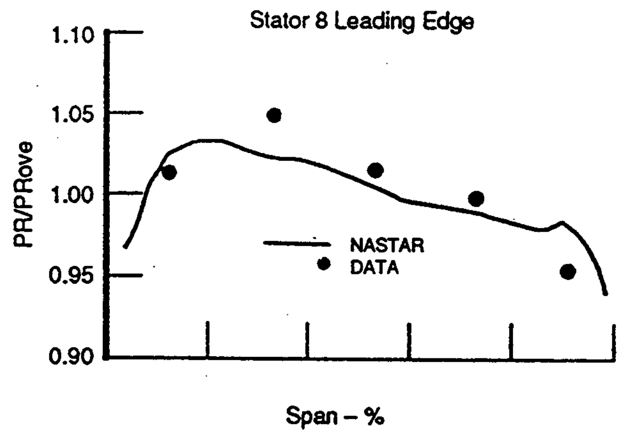

Figure 21. Total pressure profile at stator 8 leading edge.

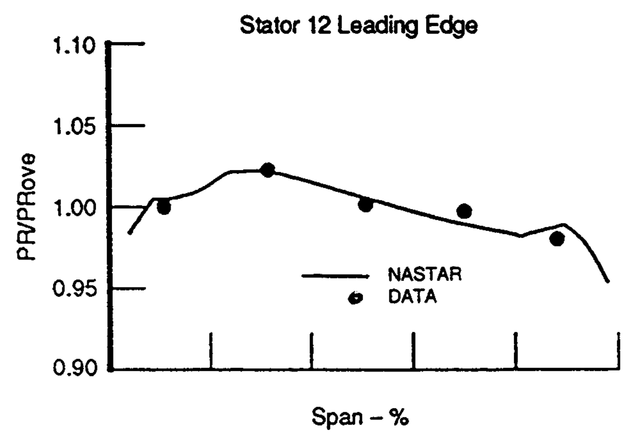

Figure 22. Total pressure profile at stator 12 leading edge.

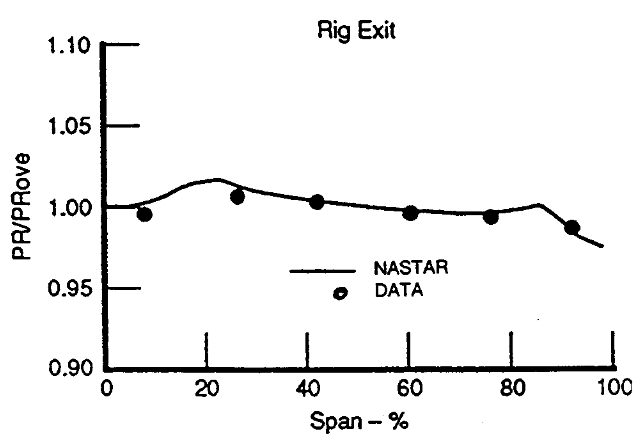

Figure 23. Total pressure profile at compressor exit.

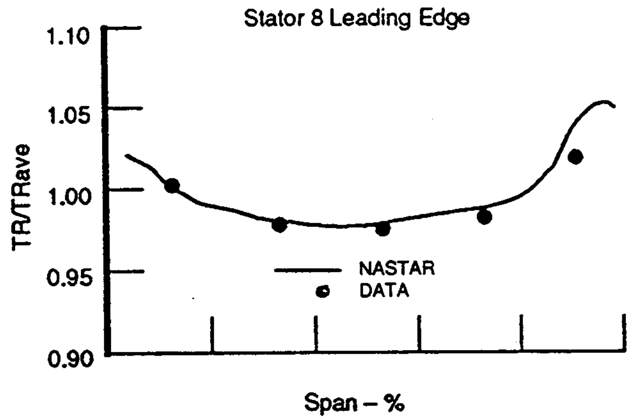

Figure 24. Total temperature profile at stator 8 leading edge.

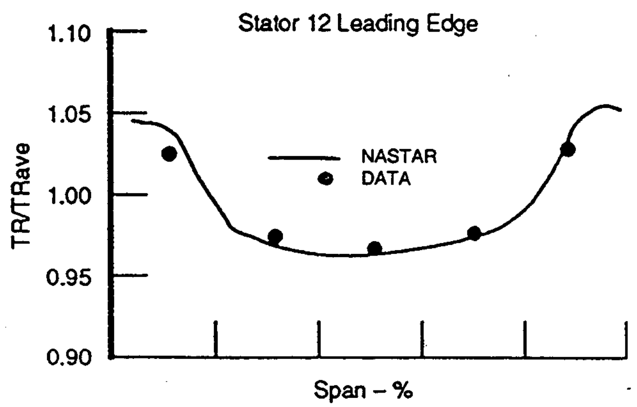

Figure 25. Total temperature profile at stator 12 leading edge.

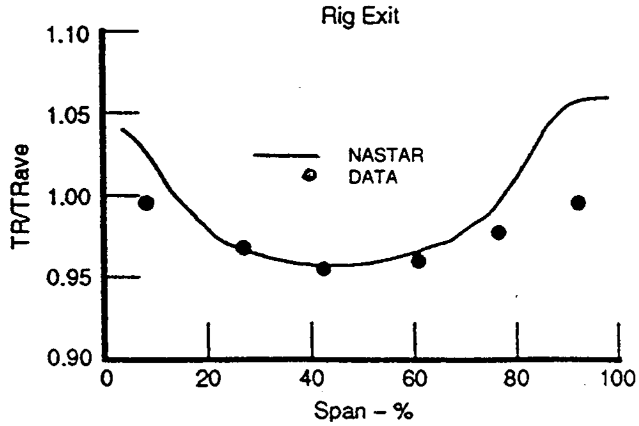

Figure 26. Total temperature profile at compressor exit.

Engine Test

Figure 27 summarizes the performance of the compressor in the engine test. The efficiency/stall margin relationship was maintained as measured in the third rig build. The 2.0% higher compressor efficiency at no overall stall margin loss has redefined the state-of-the-art performance/stall characteristics for high compressors at Pratt & Whitney. The increased compressor efficiency allows for the greater engine thrust required for the growth engine development program.

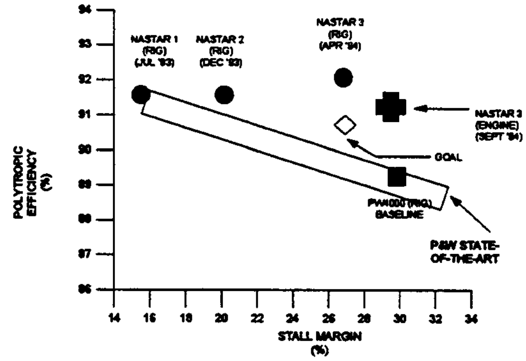

Figure 27. History of NASTAR based high pressure compressor performance, including engine test verification.

CONCLUSION

A three dimensional Navier-Stokes based design system was developed and used to design and optimize a new high pressure compressor configuration. Advanced three dimensional blading concepts, bowed stators and controlled diffusion rotor endwalls, were included in the design in order to improve compressor performance. An early version of the code used a mixing plane approach, and was successful in guiding designers in eliminating airfoil separations. The later version of the code used the bodyforce and deterministic stress technology to allow analysis off-design, where flow separations and the accurate transfer of blockage becomes important. The 3D CFD design system allowed designers to go directly to test with engine hardware in 25% of the time and 50% of the cost of a traditional empirically based design system. The new design system avoided research rig tests and full scale rig tests with variable geometry. The CFD system allowed for a state-of-the art design on the first rig build. The CFD system allowed designers to optimize the stall performance of the HPC prior to subsequent rig builds by carefully controlling the flow distributions at off-design conditions. This was done by defining, numerically testing, and optimizing mid- and rear-block stator modifications in a timely manner. The net result was a compressor design with both high efficiency and high stall margin. As a result of using CFD to numerically test new 3D airfoil concepts, the fundamental understanding of compressor aerodynamics was improved.

ACKNOWLEDGMENTS

The authors thank Pratt & Whitney management and colleagues for their support and help in developing and implementing the design system.

REFERENCES

Adamczyk, J.J., Celestina, M. L., Beach, T. A., and Barnett, M., "Simulation of Viscous Flow Within a Multistage Turbine," Trans. ASME J. of Turbomachinery, Vol. 112, 1990.

Adamczyk, Mulac, and Celestina, "A Model for Closing the Inviscid Form of the Average-Passage Equation System," ASME Journal of Turbomachinery, Vol. 108, No. 2, 1986.

Blech, Milner, Quealy and Townsend, "Turbomachinery CFD on Parallel Computers," Symposium on High-Performance Computing for Flight Vehicles and NASA TM 105932, 1992.

Chima, R., "Viscous Three-Dimensional Calculations of Transonic Fan Performance," 77th Symposium of the Propulsion and Energetics Panel Agard, 1991.

Dawes, W. N., "Towards Improved Throughflow Capability: The Use of 3D Viscous Flow Solvers in a Multistage Environment," Trans. ASME J. of Turbomachinery, Vol. 114, 1992.

Denton, J. D., "The Calculation of Three-Dimensional Viscous Flow Through Multistage Turbomachinery," Trans. ASME J. of Turbomachinery, Vol 114, 1992.

Gundy-Burlet, K., "Computations of Unsteady Multistage Compressor Flows in a Workstation Environment", ASME 91-GT-336, Orlando, Florida, 1991.

Hah and Wennerstrom, "Three-Dimensional Flowfields Inside a Transonic Compressor with Swept Blades," ASME Journal of Turbomachinery, Vol. 13, 1991.

Jennions and Turner, "Three-Dimensional Navier-Stokes Computations of Transonic Fan Using an Explicit Flow Solver and an Implicit k-e Solver," ASME Journal of Turbomachinery, Vol. 115, No. 2, 1993.

Ni, R. H., and Bogoian, J. C., "Prediction of 3D Multi-Stage Turbine Flow Field Using a Multi-Grid Euler Solver," AIAA-89-0203, 1989.

Rhie, C. M., "Pressure Based Navier-Stokes Solver Using the Multigrid Method," AIAA Journal of Propulsion and Power, pp. 564-570, Nov.-Dec. 1988.

Rhie, C. M., Zacharias, R. M., Hobbs, D. E., Sarathy, K. P., Biederman, B. P., LeJambre, C. L., and Spear, D. A., "Advanced Transonic Fan Design Procedure Based on a Navier-Stokes Method," ASME Journal of Turbomachinery, Vol. 116, No. 2, April 1994, pp. 179-346.

Rubbert, P. E., "CFD and the Changing World of Airplane Design", AIAA Wright Brothers Lecture, Anaheim, California, September 18-23, 1994.

Weingold, H., Neubert, R., Behlke, R., and Potter, G., "Reduction of Stator Endwall Losses through the Use of Bowed Stators," to be presented at The 40th ASME Gas Turbine Conference, Houston, Texas, June 5-8, 1995.